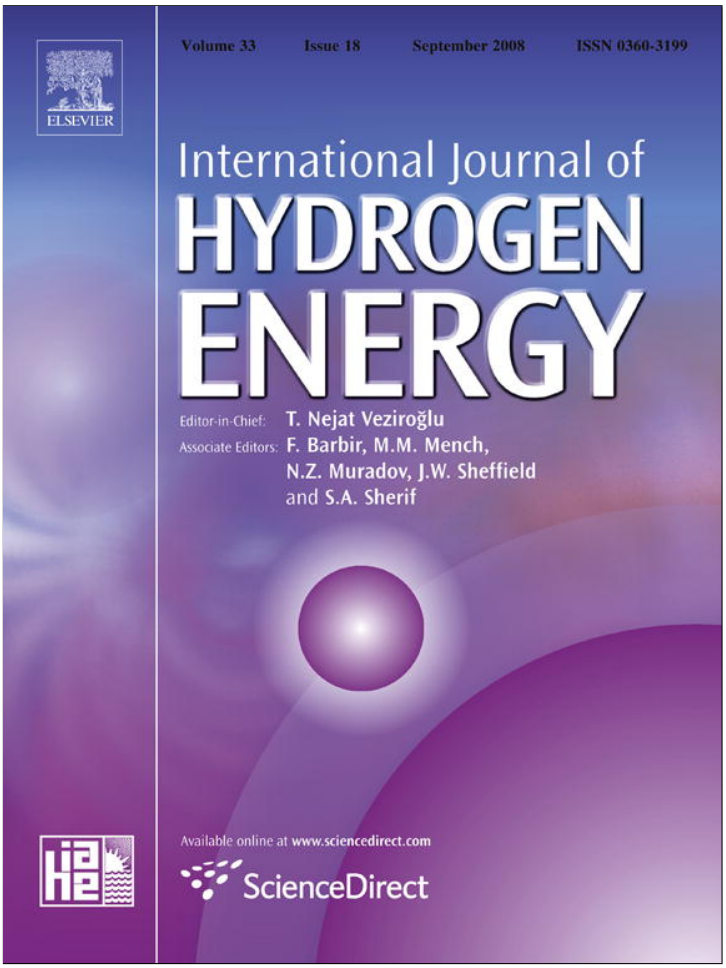

INTERNATIONAL JOURNAL OF HYDROGEN ENERGY 33 (2008) 4906–4914

Available at www.sciencedirect.com

ScienceDirect

journal homepage: www.elsevier.com/locate/he

Laminar burning velocities and combustion characteristics of propane–hydrogen–air premixed flames

Chenglong Tang, Zuohua Huang, Chun Jin, Jiajia He, Jinhua Wang, Xibin Wang, Haiyan Miao*

State Key Laboratory of Multiphase Flow in Power Engineering, Xi'an Jiaotong University, Xi'an, People's Republic of China

ARTICLE INFO

Article history:
Received 27 May 2008
Received in revised form
29 June 2008
Accepted 29 June 2008
Available online 22 August 2008

Keywords:
Propane
Hydrogen
Laminar flame
Combustion characteristics

ABSTRACT

An experimental study on laminar burning characteristics of the spherically expanding premixed propane–hydrogen–air flames was conducted at room temperature and atmospheric pressure. The unstretched laminar burning velocity, the laminar flame thickness, the Markstein number, the Zeldovich number and the global Lewis number were obtained over a range of equivalence ratios and hydrogen fractions. The influence of hydrogen addition on the laminar burning velocities and the flame front instabilities were analyzed. The results show that the unstretched laminar burning velocity increases, the laminar flame thickness decreases and the peak value of unstretched laminar burning velocity shifts to the richer mixture side with the increase of hydrogen fraction. When hydrogen fraction in the fuel is less than 60%, the Markstein number decreases with the increase of equivalence ratio, and the flame behavior is similar to that of propane–air flames. When hydrogen fraction is larger than 60%, the flame behavior is similar to that of hydrogen–air flames. At equivalence ratio less than 1.2, the Markstein number decreases with the increase of hydrogen fraction, indicating flame destabilization by hydrogen addition. At equivalence ratio larger than 1.2, the Markstein length increases with the increase of hydrogen fraction, indicating the stabilization of flame by hydrogen addition. In the case of lean mixture combustion, the Zeldovich number decreases with the increase of hydrogen addition, indicating the lowering of activation temperature of the mixture. The global Lewis number decreases with the increase of hydrogen fraction, and this indicates the increase of preferential-diffusion instabilities by hydrogen addition.

1. Introduction

Increasing concern over the fossil fuel shortage and air pollution brings an increasing study on the alternative fuels around the world community. Propane, which is a major component of liquid petroleum gas, has good air–fuel mixing potential and hence low HC and CO emissions due to its low boiling temperature. Propane can be pressurized into the liquid stage under a moderate pressure, and this makes onboard storage and handling easier [1]. Hydrogen has high flame speed, wide flammability range [2–5], low minimum ignition energy, and no emissions of HC or CO_2 [6,7]. Recent studies on internal combustion engines with hydrogen enriched fuels showed that hydrogen addition could increase engine thermal

* *Corresponding author*. School of Energy and Power Engineering, Xi'an Jiaotong University, Xi'an 710049, People's Republic of China. Tel.: +86 29 82665075; fax: +86 29 82668789.
E-mail address: zhhuang@mail.xjtu.edu.cn (Z. Huang).

0360-3199/$ – see front matter
doi:10.1016/j.ijhydene.2008.06.063

Nomenclature

X_h	volume percentage of hydrogen in fuel blends
ϕ	equivalence ratio
F/A	fuel–air ratio
α	flame stretch rate, 1/s
L_b	burned gas Markstein length, mm
ρ_u, ρ_b	unburned and burned gas densities, kg/m^3
u_n	stretched laminar burning velocity, m/s
λ	thermal conductivity of unburned gas, W/m K
L_u	unburned gas Markstein length, mm
Ze	Zeldovich number
T_{ad}	adiabatic flame temperature, K
σ	density ratio, ($\sigma = \rho_u/\rho_b$)
r_u	flame radius, mm
t	time, s
S_n	flame propagation speed, m/s
S_l	unstretched flame propagation speed, m/s
A	flame area, m^2
u_l	unstretched laminar burning velocity, m/s
δ_l	laminar flame thickness, mm
C_p	specific heat of unburned gas, kJ/kg K
Ma	Markstein number, ($Ma = L_u/\delta_l$)
f^0	mass burning flux, ($f^0 = \rho_u u_l$)
T_u	initial temperature, K
Le	global flame Lewis number

efficiency, improve lean burn capability and mitigate the global warming problem [6,8–11]. Fundamental combustion characteristics of propane–air [12–15] and hydrogen–air [16–18] mixtures have been extensively studied. However, few reports on combustion characteristics of hydrogen enriched propane–air flames were presented. Milton and Keck measured the laminar burning velocities of the stoichiometric hydrogen–propane–air flames [19]. Yu et al. studied the laminar burning characteristics of propane–hydrogen–air flames with the assumption that the stoichiometrically small amounts of hydrogen in the mixture was completely consumed and found a linear correlation of laminar burning velocity with the hydrogen concentration [20]. Law and Kwon studied the potential of hydrocarbon addition to suppress explosion hazards and found that a small or moderate amount of propane addition could remarkably reduce the laminar burning velocities and would suppress the propensity of onset of both diffusional-thermal and hydrodynamic cellular instabilities in hydrogen–air flames [21]. Law et al. investigated the phenomenon of spontaneous cell formation on expanding lean hydrogen spherical flames with propane addition to retard the reaction intensity and found that the critical radius for onset of instability increased with the increase of propane fraction [22].

Laminar burning velocity is one of the most important parameters in combustion because the laminar burning velocity is a physiochemical property of a combustible mixture. Accurate laminar burning velocity values can be used to validate the chemical reaction mechanisms [17,23] and is of practical importance in the design and analysis of internal combustion engines and power plant burners [19]. There are three methods to measure the laminar burning velocity: The stagnation plane flame method [13,20], the heat flux method [14,24] and the combustion bomb method [12,15,23]. The stagnation plane flame method can establish different flame configurations, but it is difficult to draw a clear flame front and to stabilize the flame under the high-pressure conditions. The heat flux method needs to determine the heat loss as a function of the inlet velocity and to extrapolate the results to zero heat loss to get the adiabatic burning velocity. The combustion bomb method utilizes the prototypical propagating spherical flame configuration and has drawn particular attention due to its simple flame configuration, well-defined flame stretch rate and well-controlled experimentation [25,26]. In this study, the laminar burning velocities of the propane–hydrogen–air mixtures were measured by using the spherically expanding flame.

Except for the plane one-dimensional unstretched flame, the actual flames such as the Bunsen burner flame, the counterflow flame or the propagating spherical flame are always embedded with the positive and/or the negative flame stretch. The laminar flame speeds' response to the stretch in the curved areas of the flame was investigated by Markstein [27], Manton, von Elbe and Lewis [28], Parlange [29] and Bechtold [30] and the studies showed that the burning velocity in the curved region was reduced and the stretch tended to stabilize the flame if the excess constituent possesses large diffusivity. The opposite nonequidiffusive behavior for the lean and rich flames of propane–air and hydrogen–air was well established [16,26,31]. However, quantitative description of combustion characteristics of laminar propane–hydrogen–air flame response to flame stretch has not been reported so far. In this study, the outwardly propagating spherical flame was used to obtain the laminar burning parameters, including the unstretched laminar burning velocity (u_i) and the laminar flame thickness (δ_l) which can be directly determined from the flame solution [26,32,33], the Markstein length (L_b and/or L_u) or Markstein number (Ma), which represent the sensitivity of flame stability response to flame stretch [25], the Zeldovich number (Ze), and hence the one-step overall activation energy (E_a), which can be extracted from the dependence of u_i on the adiabatic flame temperature (T_{ad}) [31,34,35], and the global flame Lewis number (Le), which has been conventionally estimated for sufficiently off-stoichiometric mixtures from the freestream values of the mixture properties. It was pointed out in Refs. [31] and [36] that since transport properties were fairly strongly dependent on temperature and mixture composition, which vary significantly across the flame, Le is a global flame property and as such should be extracted from the flame response.

2. Experimental setup and procedures

The volume percentage of hydrogen in fuel blends (X_h) is

$$X_h = \frac{V_H}{V_H + V_C} \times 100 \quad (1)$$

where V_H and V_C are the volume fraction of hydrogen and propane in the fuel blends, respectively.

The overall equivalence ratio (ϕ) is defined as

$$\phi = \frac{F/A}{(F/A)_{st}} \quad (2)$$

where (F/A) is the fuel–air ratio and $(F/A)_{st}$ refers to the stoichiometric value of (F/A). For the stoichiometric propane–air and hydrogen–air mixture combustion

$$C_3H_8 + 5(O_2 + 3.76N_2) \rightarrow 3CO_2 + 4H_2O + 5 \times 3.76N_2 \quad (3)$$

$$H_2 + 0.5(O_2 + 3.76N_2) \rightarrow H_2O + 0.5 \times 3.76N_2 \quad (4)$$

Mixture can be expressed as $\{(1 - X_h\%)C_3H_8 + X_h\%H_2\} + \text{air}$. From Eqs. (3) and (4), the stoichiometric fuel–air ratio can be expressed as

$$(F/A)_{st} = \frac{1}{(1 - X_h\%) \times 5(1 + 3.76) + X_h\% \times 0.5(1 + 3.76)} \quad (5)$$

From Eqs. (2) and (5), the ratio of partial pressure of fuel and air can be deduced as

$$P_F/P_A = F/A = \phi \times (F/A)_{st} \quad (6)$$

As shown in Fig. 1, the experimental apparatus consists of the combustion vessel, the heating system, the ignition system, the data acquisition system and the high-speed schlieren photography system. Fig. 2 shows the schematic diagram of the cylinder-type combustion vessel with diameter of 180 mm and length of 210 mm. Two sides of the vessel are mounted with the quartz windows to allow the optical access. A high-speed digital camera operating at 10,000 frames per second was used to record the flame pictures during the flame propagation. A Kistler pressure transducer was used to record the combustion pressure. The mixtures were prepared by introducing each component according to its corresponding partial pressure for the specified overall equivalence ratio. The mixtures are ignited by the centrally located electrodes. A standard capacitive discharge ignition system is used to produce the spark. Once the combustion was completed, the combustion vessel was vacuumed and flushed with dry air for three times to avoid the influence of the residual gas on the next experiment. A time interval of 5 min was adopted to allow the mixtures to be quiescent and to avoid the influence of wall temperature. Time interval of 30 min was tested, and no appreciable difference was observed compared to the time interval of 5 min. As the flame develops in a spherical pattern, the flame radius is scaled from the flame photo recorded by the high-speed camera. Purities of propane and hydrogen in the study are 99.96% and 99.99%, respectively.

3. Laminar burning characteristics

3.1. Laminar burning velocity and Markstein number

The flame propagation speed (S_n) is the velocity of the flame front relative to a fixed position. For the outwardly propagating flames, S_n is derived from flame radius versus time data [25,32,33,37] as

$$S_n = \frac{dr_u}{dt} \quad (7)$$

where r_u is the flame radius in the schlieren photos, and t is the time.

Flame stretch rate (α) represents the expanding rate of flame area (A). In a quiescent mixture, it is defined as

$$\alpha = \frac{d(\ln A)}{dt} = \frac{2}{r_u}\frac{dr_u}{dt} = \frac{2}{r_u}S_n \quad (8)$$

In the early stage of flame propagation where the pressure does not vary significantly yet, there exists a linear relationship between the flame propagation speed and the stretch rate; that is

$$S_l - S_n = L_b\alpha \quad (9)$$

The unstretched propagation speed, S_l, can be obtained as the intercept value at $\alpha = 0$, in the plot of S_n against α. The burned gas Markstein length, L_b, is the slope of $S_n - \alpha$ fitting curve.

In the early stage of flame propagation, the flame undergoes an isobaric developing process, the unstretched laminar burning velocity, u_l, is related to S_l from mass conservation across the flame front

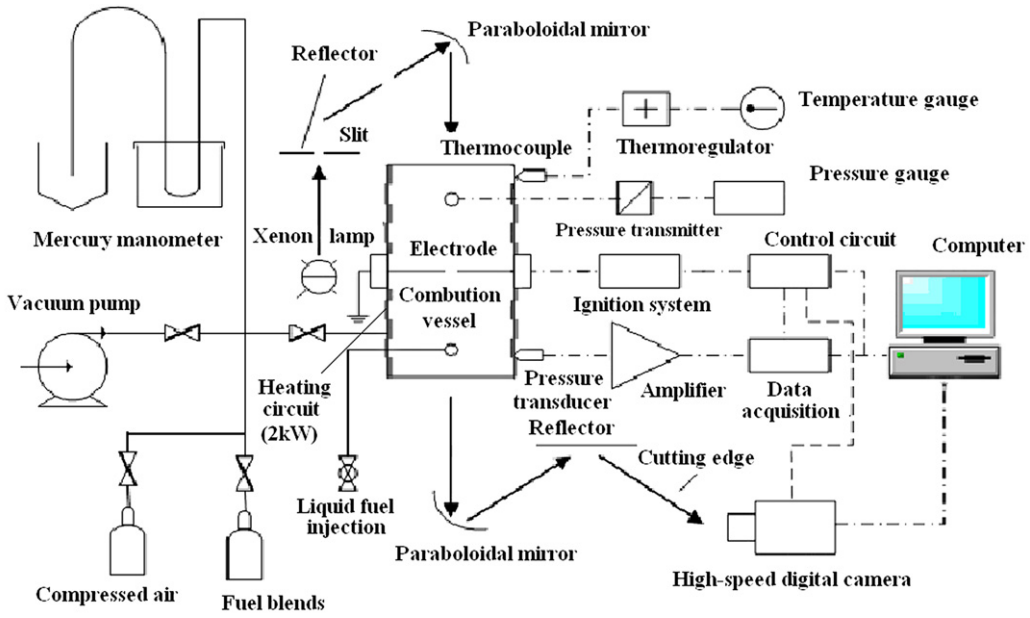

Fig. 1 – Experimental setup.

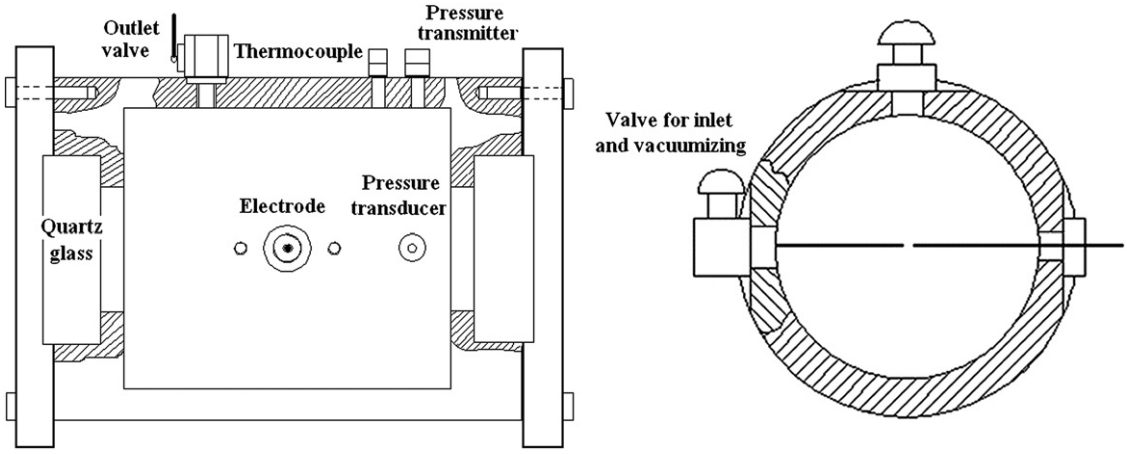

Fig. 2 – Schematic of the combustion vessel.

$$A\rho_u u_l = A\rho_b S_l \tag{10}$$

where A is the flame front area, ρ_u and ρ_b are the unburned and burned gas density, respectively. Together with the adiabatic temperature (T_{ad}) in the following section, ρ_u and ρ_b were obtained by the Equilibrium model with CHEMKIN. The unstretched laminar burning velocity, u_l, can be obtained from Eq. (10)

$$u_l = \rho_b S_l/\rho_b \tag{11}$$

Bradley defined the stretched laminar burning velocity (u_n) as the consumption rate of the unburned gas mixture [25,34]

$$u_n = S\left[S_n\frac{\rho_b}{\rho_u}\right] \tag{12}$$

where S is a generalized function that depends upon the flame radius and the density ratio, and accounts for the effect of flame thickness on the mean density of the burned gases [25,34]. The generalized expression of S is

$$S = 1 + 1.2\left[\frac{\delta_l}{r_u}\left(\frac{\rho_u}{\rho_b}\right)^{2.2}\right] - 0.15\left[\frac{\delta_l}{r_u}\left(\frac{\rho_u}{\rho_b}\right)^{2.2}\right]^2 \tag{13}$$

In this study, the laminar flame thickness δ_l is determined with the suggestion of Law et al. [22,38]

$$\delta_l = (\lambda/C_p)/(\rho_u u_l) \tag{14}$$

Here, λ and C_p are the unburned gas thermal conductivity and the specific heat, respectively.

The unburned gas Markstein length (L_u) can be obtained by the linear relationship between laminar burning velocity and stretch rate

$$u_l - u_n = L_u\alpha \tag{15}$$

Markstein number is obtained by nondimensionalizing L_u with δ_l

$$Ma = L_u/\delta_l \tag{16}$$

3.2. *Zeldovich number and Lewis number*

Zeldovich number (Ze) is a dimensionless form of the overall activation energy. It reflects the mass burning flux (f^0) dependence on the activation temperature. The activation energy (E_a) can be extracted from the dependence of mass burning flux on the adiabatic temperature (T_{ad}), as suggested by Jomaas et al. [31], Egolfopoulos and Law [35] and Clavin [39]

$$\frac{E_a}{R} = -2\frac{d\left(\ln\left(f^0\right)\right)}{d(1/T_{ad})} \tag{17}$$

$$Ze = \frac{E_a}{R}\frac{T_{ad} - T_u}{T_{ad}^2} \tag{18}$$

Here, $f^0 = \rho_u u_l$, T_u is the unburned gas temperature and R is the universal gas constant.

The global flame Lewis number (Le) can be extracted from the following equation as suggested by Jomaas et al. [31] and Clavin [39]

$$Ma = \frac{\sigma}{\sigma - 1}\left[\frac{Ze(Le-1)}{2}\int_0^{1-1/\delta}\frac{\ln(1+x)}{x}dx + \ln(\sigma)\right] \tag{19}$$

Here, $\sigma = \rho_u/\rho_b$ is the density ratio and x is a dummy variable.

4. Results and discussions

4.1. *Flame propagation speed and burned gas Markstein length*

In the experiment, the homogeneous mixture in the combustion vessel was ignited by the centrally located electrodes. The spark energy and electrodes can affect the flame propagation in the early stage. Bradley et al. showed that the region due to the influence of spark energy and electrodes is within 5 mm of the flame radius [22]. Together with the consideration of isobaric combustion, the data used in the analysis are limited within the flame radius ranging from 5 mm to 25 mm.

Fig. 3 shows flame radii versus the time of the stoichiometric propane–hydrogen–air flames. There exists a linear relationship between the flame radius and time except for the case of the flame radius less than 5 mm where the flame propagation is influenced by ignition energy and electrodes. With the increase of hydrogen fraction, the slope of the

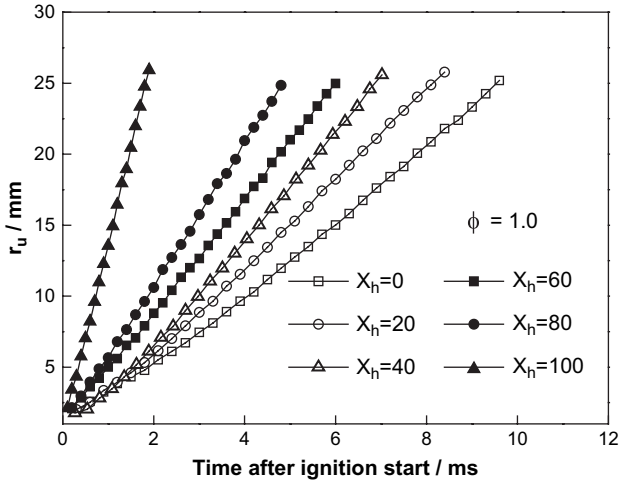

Fig. 3 – Flame radii versus time.

radius–time line increases, indicating the increase of the flame propagation speed. Fig. 4 gives the flame propagation speed (S_n) versus flame radius at the equivalence ratio of 1.0. For various hydrogen addition levels, S_n slightly increases with the propagation of the flame. With the increase of hydrogen fraction, the flame propagation speed increases and the increment of the flame propagation speed becomes larger with the increase of hydrogen fraction especially when hydrogen fraction in the fuel blends is larger than 80%.

Fig. 5 gives the flame propagation speed versus the flame stretch rate under the leaner mixture ($\phi = 0.6$) and the richer mixture ($\phi = 1.6$). The flame propagation speed increases with the increase of hydrogen fraction for both the lean flame and the rich flame. In the case of lean propane–hydrogen–air flame ($\phi = 0.6$), the slope of $S_n - \alpha$ fitting curve changes from a negative value to a positive value and the burned gas Markstein length (L_b) decreases from a positive value to a negative value with the increase of hydrogen fraction, and this reflects flame destabilization as hydrogen is added. In the case of rich flame ($\phi = 1.6$), the slope of $S_n - \alpha$ fitting curve changes from a positive value to a negative value and the burned gas Markstein length (L_b) changes from a negative value to a positive value with the increase of hydrogen fraction, and this indicates flame stabilization as hydrogen is added. This phenomenon results from the opposite diffusion behavior of propane and hydrogen. The diffusivity of propane is lower than that of air and the diffusivity of hydrogen is higher than that of air. For the lean mixture, the propane–air flame tends to be stable and the hydrogen–air flames tends to be unstable, and increasing hydrogen fraction would lead to destabilization of the flame; and for rich mixture, the propane–air flame tends to be unstable and the hydrogen–air flames tends to be stable, and increasing hydrogen fraction would lead to stabilization of the flame [27,28,30].

Fig. 6 shows the unstretched flame propagation speed (S_l) with equivalence ratio at different hydrogen fractions. When X_h is less than 80, the curve of S_l versus equivalence ratio at different X_h shows a similar pattern with the peak value at the equivalence ratio of 1.2. For hydrogen–air combustion ($X_h = 100$), the unstretched flame propagation speed increases monotonically with the increase of equivalence ratio. With the increase of hydrogen fraction, the maximum value of S_l shifts to the richer mixture side. For a given equivalence ratio, S_l increases with the increase of X_h and the increment becomes larger when X_h is larger than 80, that is, the

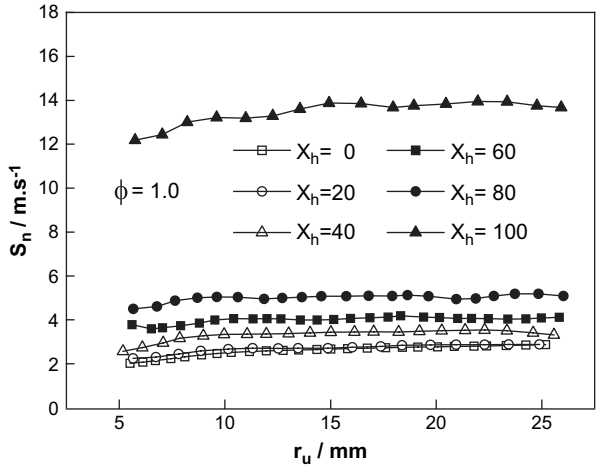

Fig. 4 – Flame propagation speed versus flame radius.

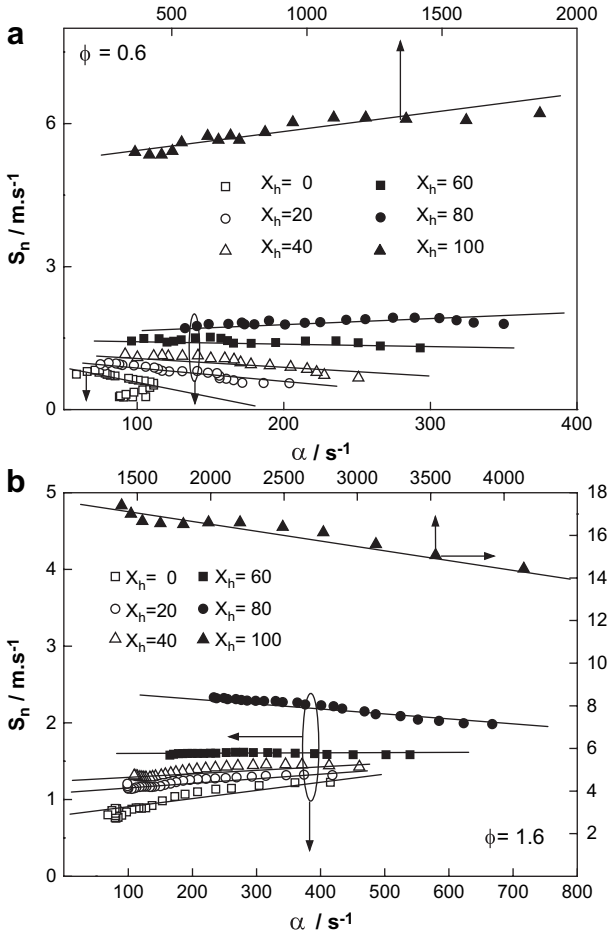

Fig. 5 – Flame propagation speed versus flame stretch rate.

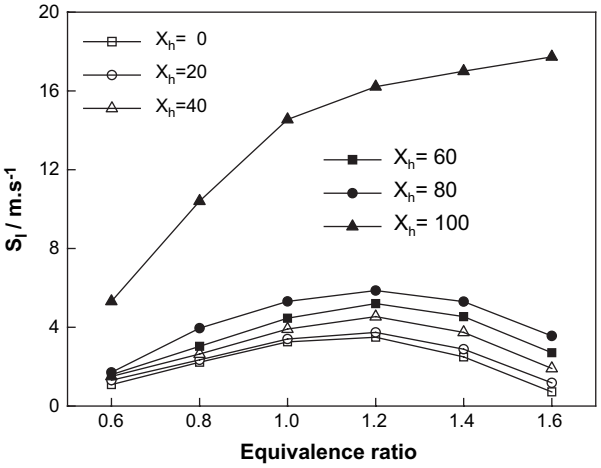

Fig. 6 – S_l versus equivalence ratio at different X_h.

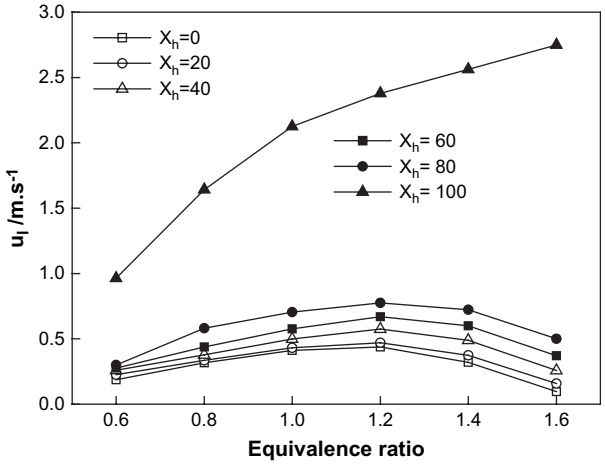

Fig. 8 – u_l versus equivalence ratio at different X_h.

increment of S_l from X_h of 80 to X_h of 100 is three or four times that from X_h of 0 to X_h of 80.

Fig. 7 gives the burned gas Markstein length versus the equivalence ratio at different hydrogen fractions. When $X_h < 60$, L_b decreases monotonically with the increase of equivalence ratio, indicating the increase of flame front instability. When $X_h > 60$, L_b increases monotonically with the increase of equivalence ratio, and this indicates the decrease of flame front instability. This behavior is result of the competition of the nonequidiffusion of propane and hydrogen. When $X_h < 60$, propane is the dominant component that determines the stability and the flame behavior is similar to that of propane flame. When $X_h > 60$, hydrogen becomes the dominant component that determines flame stability and the flame behavior is similar to that of hydrogen flame. The behavior of L_b with the increase of X_h is different at different equivalence ratios. When $\phi < 1.2$, L_b decreases with the increase of X_h, suggesting the decrease of flame front stability as hydrogen is added. When $\phi > 1.2$, L_b increases with the increase of X_h, indicating the increase of flame front stability as hydrogen is added.

4.2. *Laminar burning velocity and Markstein number*

Fig. 8 shows the unstretched laminar burning velocity versus the equivalence ratio at different hydrogen fractions. Similar to the unstretched flame propagation speed, when X_h is less than 80, with the increase of equivalence ratio, the curves show similar pattern with the peak value at the equivalence ratio of 1.2. For hydrogen combustion ($X_h = 100$), the unstretched laminar burning velocity increases monotonically with the increase of equivalence ratio. Remarkable increase of the unstretched laminar burning velocity is observed when X_h is over 80. With the increase of hydrogen fraction, the maximum value of u_l shifts to the richer mixture side.

Fig. 9 gives the laminar flame thickness δ_l versus the equivalence ratio at different hydrogen fractions. The lowest value of δ_l appears at the equivalence ratio of 1.2 except for hydrogen–air mixture. For a given equivalence ratio, δ_l decreases with the increase of X_h and the decreasing tendency becomes more apparent when X_h is over 80.

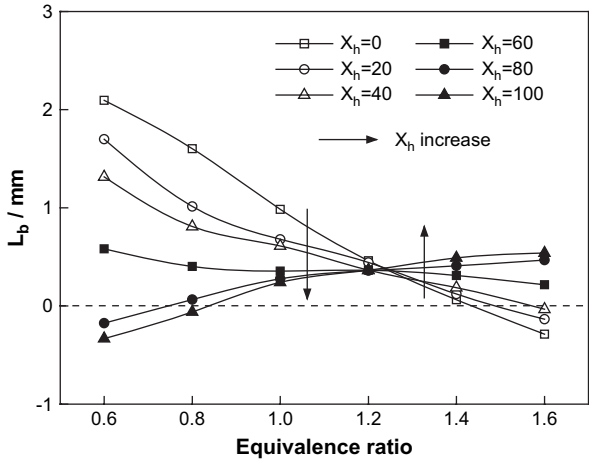

Fig. 7 – L_b versus equivalence ratio at different X_h.

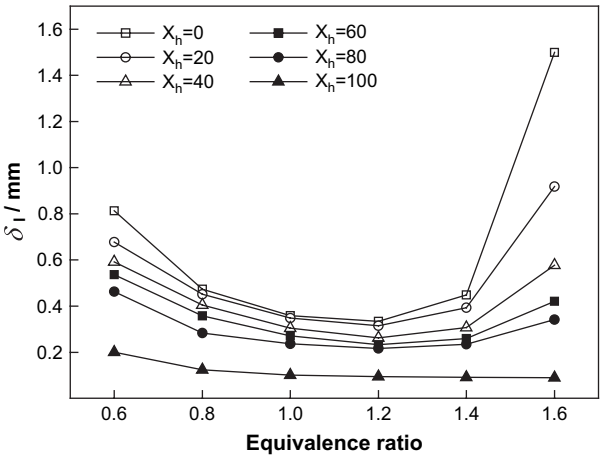

Fig. 9 – Laminar flame thickness versus equivalence ratio at different X_h.

Fig. 10 gives the unburned gas Markstein length and the Markstein number versus the equivalence ratio at different hydrogen fractions. When $X_h < 60$, both L_u and Ma decrease with the increase of equivalence ratio. When $X_h > 60$, both L_u and Ma increase with the increase of equivalence ratio. When $\phi < 1.2$, both L_u and Ma decrease with the increase of X_h, reflecting the flame destabilization as hydrogen is added. When $\phi > 1.2$, both L_u and Ma increase with the increase of X_h, and this reflects the flame stabilization as hydrogen is added. The behavior of L_b to mixture composition (ϕ and/or X_h) is consistent to that of L_u and this proves the consistency of the two definitions of Markstein lengths in reflecting the flame front stabilities.

4.3. *Global flame Lewis number*

Fig. 11 gives the adiabatic temperature (T_{ad}) versus X_h at the equivalence ratios of 0.6, 0.8 and 1.0. When $X_h < 80$, there is a slight increase of T_{ad} with the increase of X_h. When X_h is larger than 80, T_{ad} increases remarkably with the increase of X_h. The volumetric heating value of hydrogen is lower than that of propane, but the fuel–air ratio of hydrogen is 10 times that of propane at the stoichiometric condition, (as shown in Eqs. (3) and (4)), thus increasing X_h will decrease the amount of air in which nitrogen is a major component and determines

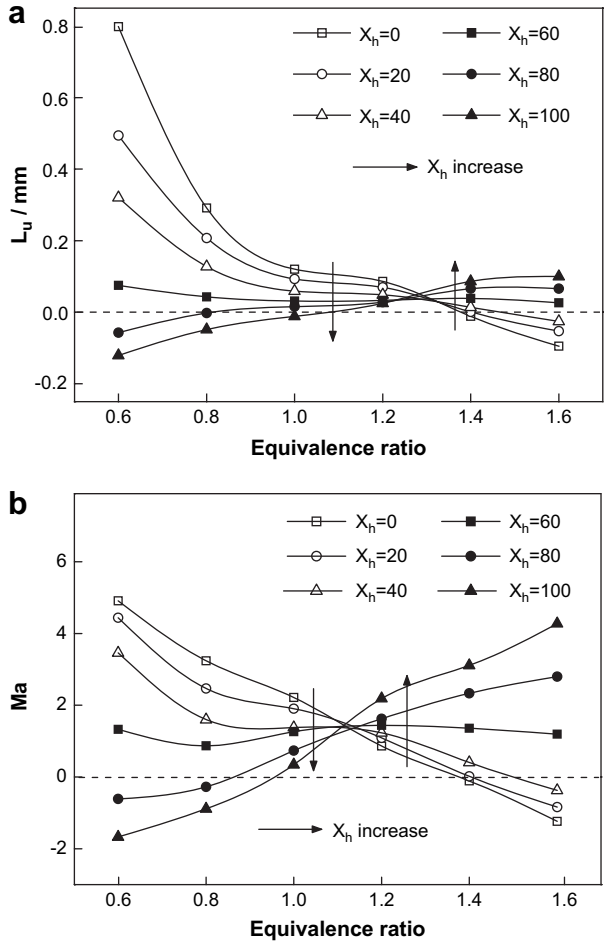

Fig. 10 – L_u and Ma versus equivalence ratio at different X_h.

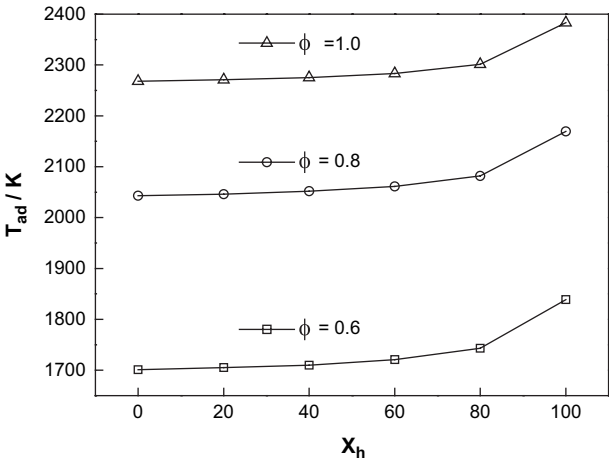

Fig. 11 – T_{ad} versus X_h at different equivalence ratios.

the specific heat of the mixture. Fig. 12 gives the mass burning flux (f^0) versus X_h at the equivalence ratios of 0.6, 0.8 and 1.0. f^0 increases with the increase of X_h and the behavior becomes remarkable when X_h is over 80. The characteristics of mass burning flux is strongly related to the laminar burning velocity which gives the same behavior to X_h and ϕ.

Fig. 13 gives the Zeldovich number (Ze) versus X_h at the equivalence ratios of 0.6, 0.8 and 1.0. Ze shows a slight decrease with the increase of X_h when $X_h < 80$, and Ze decreases remarkably with the increase of X_h when $X_h > 80$. The decrease of Ze reflects the decrease in the global activation energy. This behavior reflects the controlling influence of adiabatic flame temperature, which increases with the increase of X_h and facilitates the temperature-sensitive two-body branching reactions relative to the temperature-insensitive three-body termination reactions [31], leading to faster reactions with the increase of X_h. It should be pointed out that the values of Ze at $\phi = 1.0$ as shown by the closed triangle in Fig. 13 is also calculated from Eq. (17) which holds only for sufficiently off-stoichiometric mixtures for which the reaction rate is controlled by the deficient reactant [31]. Thus this line

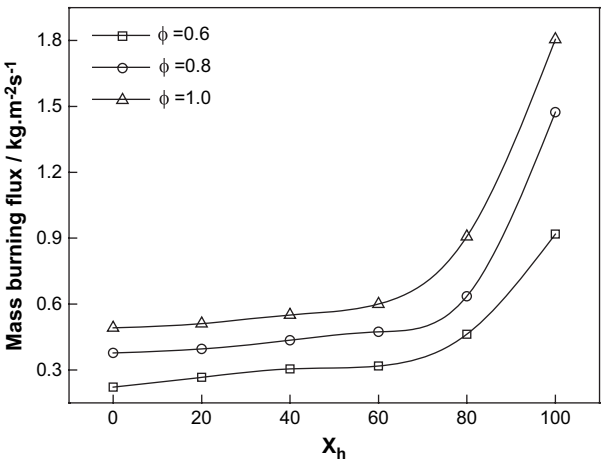

Fig. 12 – Mass burning flux versus X_h at different equivalence ratios.

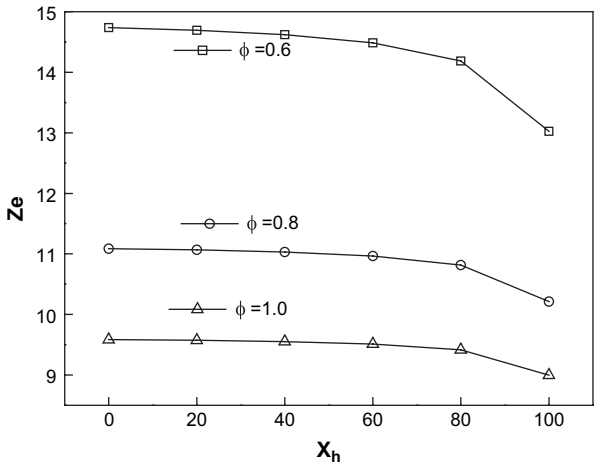

Fig. 13 – Zeldovich number versus X_h at different equivalence ratios.

only provides the reference to the analysis of *Ze* rather than quantitatively.

Fig. 14 gives the global flame Lewis number (*Le*) versus X_h at the equivalence ratios of 0.6, 0.8 and 1.0. At equivalence ratios of 0.6 and 0.8, *Le* shows a slight decrease with the increase of X_h when $X_h < 80$ and *Le* decreases significantly with the increase of X_h when $X_h > 80$. This indicates that the preferential-diffusion instability is promoted with increasing hydrogen under lean mixture condition. For the stoichiometric mixture combustion, although *Le* slightly decreases with the increase of X_h, the values at different hydrogen fractions are close to unity, indicating the neutral flame front stability. The effective Lewis number given by Law in Ref. [22] at 5 atm and equivalence ratio $\phi' = 0.8$ is also plotted in Fig. 14 for the comparison. Although the effective Lewis number by Law is at the higher initial pressure, the data can still be comparable since Lewis number is less dependent on pressure because increasing pressure increases density but decreases the diffusivity. In addition, the definition of hydrogen mixing ratio and equivalence ratio in Ref. [22] is different from the definitions in this work but this difference does not exist for pure propane ($X_h = 0$) or hydrogen ($X_h = 100$). Taking into consideration of the insensitivity of Lewis number on pressure and the difference in defining the hydrogen fraction and equivalence ratio, *Le* number demonstrated in this paper at pure propane ($X_h = 0$) and pure hydrogen ($X_h = 100$) reflects the same value as that in Ref. [22].

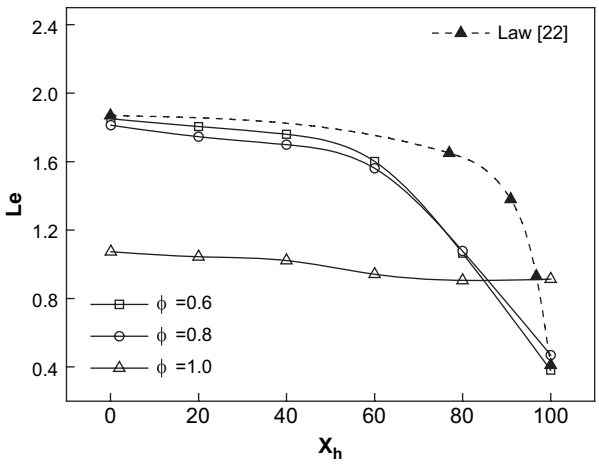

Fig. 14 – Lewis number versus X_h at different equivalence ratios.

5. Conclusions

An experimental study on the spherically expanding laminar premixed propane–hydrogen–air flames was conducted at room temperature and atmospheric pressure. The main conclusions are summarized as follows.

1. The unstretched flame propagation speed and the unstretched laminar burning velocity increase with the increase of hydrogen fraction in the fuel blends, and the increasing tendency becomes more remarkable at large hydrogen fraction, the peak value of the unstretched flame propagation speed and the unstretched laminar burning velocity shift to the rich mixture side with the increase of hydrogen fraction in the fuel blends.
2. When the hydrogen fraction is less than 60%, the Markstein length and the Markstein number decrease with the increase of equivalence ratio and the flame stability behavior is similar to that of propane–air flames. When hydrogen fraction is larger than 60%, the Markstein length and the Markstein number increase with the increase of equivalence ratio and the flame stability behavior is similar to that of hydrogen–air flames. When the equivalence ratio is less than 1.2, the Markstein length and the Markstein number decrease with the increase of hydrogen fraction, indicating the flame destabilization by hydrogen addition. When the equivalence ratio is larger than 1.2, the Markstein length and the Markstein number increase with the increase of hydrogen fraction, indicating the flame stabilization by hydrogen addition.
3. For lean mixture combustion, Lewis number decreases with the increase of hydrogen fraction and the decreasing trend becomes more obvious at large hydrogen fraction, indicating the increase in the preferential-diffusion instability with hydrogen addition.

Acknowledgement

The study is supported by the National Natural Science Foundation of China (50636040, 50521604), National Basic Research Program (2007CB210006).

REFERENCES

[1] Yap D, Karlovsky J, Megaritis A, Wyszynski ML, Xu H. An investigation into propane homogeneous charge

compression ignition (HCCI) engine operation with residual gas trapping. Fuel 2005;84(18):2372–9.
[2] Wang J, Huang Z, Miao H, Wang X, Jiang D. Characteristics of direct injection combustion fuelled by natural gas-hydrogen mixtures using a constant volume vessel. International Journal of Hydrogen Energy 2008;33(7):1947–56.
[3] Ilbas M, Crayford AP, Yilmaz I, Bowen PJ, Syred N. Laminar-burning velocities of hydrogen-air and hydrogen-methane-air mixtures: An experimental study. International Journal of Hydrogen Energy 2006;31(12):1768–79.
[4] Wierzba I, Wang Q. The flammability limits of H_2–CO–CH_4 mixtures in air at elevated temperatures. International Journal of Hydrogen Energy 2006;31(4):485–9.
[5] Wierzba I, Kilchyk V. Flammability limits of hydrogen–carbon monoxide mixtures at moderately elevated temperatures. International Journal of Hydrogen Energy 2001;26(6):639–43.
[6] do Sacramento EM, de Lima LC, Oliveira CJ, Veziroglu TN. A hydrogen energy system and prospects for reducing emissions of fossil fuels pollutants in the Cear? state–Brazil. International Journal of Hydrogen Energy 2008;33(9):2132–7.
[7] Granovskii M, Dincer I, Rosen MA. Greenhouse gas emissions reduction by use of wind and solar energies for hydrogen and electricity production: economic factors. International Journal of Hydrogen Energy 2007;32(8):927–31.
[8] Van Blarigan P, Keller JO. A hydrogen fuelled internal combustion engine designed for single speed/power operation. International Journal of Hydrogen Energy 1998; 23(7):603–9.
[9] Huang Z, Wang J, Liu B, Zeng K, Yu J, Jiang D. Combustion characteristics of a direct-injection engine fueled with natural gas–hydrogen blends under different ignition timings. Fuel 2007;86(3):381–7.
[10] Wang J, Huang Z, Fang Y, Liu B, Zeng K, Miao H, et al. Combustion behaviors of a direct-injection engine operating on various fractions of natural gas-hydrogen blends. International Journal of Hydrogen Energy 2007; 32(15):3555–64.
[11] Saravanan N, Nagarajan G. An experimental investigation of hydrogen-enriched air induction in a diesel engine system. International Journal of Hydrogen Energy 2008;33(6):1769–75.
[12] Tseng LK, Ismail MA, Faeth GM. Laminar burning velocities and Markstein numbers of hydrocarbon/air flames. Combustion and Flame 1993;95(4):410–26.
[13] Vagelopoulos CM, Egolfopoulos FN. Direct experimental determination of laminar flame speeds. Symposium (International) on Combustion 1998;27(1):513–9.
[14] Bosschaart KJ, de Goey LPH, Burgers JM. The laminar burning velocity of flames propagating in mixtures of hydrocarbons and air measured with the heat flux method. Combustion and Flame 2004;136(3):261–9.
[15] Marley SK, Roberts WL. Measurements of laminar burning velocity and Markstein number using high-speed chemiluminescence imaging. Combustion and Flame 2005; 141(4):473–7.
[16] Kwon S, Tseng LK, Faeth GM. Laminar burning velocities and transition to unstable flames in $H_2/O_2/N_2$ and $C_3H_8/O_2/N_2$ mixtures. Combustion and Flame 1992;90(3–4):230–46.
[17] Aung KT, Hassan MI, Faeth GM. Flame stretch interactions of laminar premixed hydrogen/air flames at normal temperature and pressure. Combustion and Flame 1997; 109(1–2):1–24.
[18] Kwon OC, Faeth GM. Flame/stretch interactions of premixed hydrogen-fueled flames: measurements and predictions. Combustion and Flame 2001;124(4):590–610.
[19] Milton BE, Keck JC. Laminar burning velocities in stoichiometric hydrogen and hydrogen–hydrocarbon gas mixtures. Combustion and Flame 1984;58(1):13–22.
[20] Yu G, Law CK, Wu CK. Laminar flame speeds of hydrocarbon + air mixtures with hydrogen addition. Combustion and Flame 1986;63(3):339–47.
[21] Law CK, Kwon OC. Effects of hydrocarbon substitution on atmospheric hydrogen–air flame propagation. International Journal of Hydrogen Energy 2004;29(8):867–79.
[22] Law CK, Jomaas G, Bechtold JK. Cellular instabilities of expanding hydrogen/propane spherical flames at elevated pressures: theory and experiment. Proceedings of the Combustion Institute 2005;30(1):159–67.
[23] Huzayyin AS, Moneib HA, Shehatta MS, Attia AMA. Laminar burning velocity and explosion index of LPG-air and propane-air mixtures. Fuel 2007;87(1):39–57.
[24] Bosschaart KJ, de Goey LPH. Detailed analysis of the heat flux method for measuring burning velocities. Combustion and Flame 2003;132(1–2):170–80.
[25] Bradley D, Gaskell PH, Gu XJ. Burning velocities, Markstein lengths, and flame quenching for spherical methane–air flames: a computational study. Combustion and Flame 1996; 104(1–2):176–98.
[26] Sun CJ, Sung CJ, He L, Law CK. Dynamics of weakly stretched flames: quantitative description and extraction of global flame parameters. Combustion and Flame 1999;118(1–2):108–28.
[27] Markstein GH. Nonisotropic propagation of combustion waves. The Journal of Chemical Physics 1952;20(6):1051–2.
[28] Manton J, von Elbe G, Lewis B. Nonisotropic propagation of combustion waves in explosive gas mixtures and the development of cellular flames. The Journal of Chemical Physics 1952;20(1):153–7.
[29] Parlange JY. Influence of preferential diffusion on the stability of a laminar flame. The Journal of Chemical Physics 1968;48(4):1843–9.
[30] Bechtold JK, Matalon M. Hydrodynamic and diffusion effects on the stability of spherically expanding flames. Combustion and Flame 1987;67(1):77–90.
[31] Jomaas G, Law CK, Bechtold JK. On transition to cellularity in expanding spherical flames. Journal of Fluid Mechanics 2007; 583:1–26.
[32] Huang Z, Wang Q, Yu J, Zhang Y, Zeng K, Miao H, et al. Measurement of laminar burning velocity of dimethyl ether-air premixed mixtures. Fuel 2007;86(15):2360–6.
[33] Huang Z, Zhang Y, Zeng K, Liu B, Wang Q, Jiang D. Measurements of laminar burning velocities for natural gas-hydrogen-air mixtures. Combustion and Flame 2006; 146(1–2):302–11.
[34] Bradley D, Hicks RA, Lawes M, Sheppard CGW, Woolley R. The measurement of laminar burning velocities and Markstein Numbers for iso-octane-air and iso-octane-n-heptane-air mixtures at elevated temperatures and pressures in an explosion bomb. Combustion and Flame 1998;115(1–2):126–44.
[35] Egolfopoulos FN, Law CK. Chain mechanisms in the overall reaction orders in laminar flame propagation. Combustion and Flame 1990;80(1):7–16.
[36] Sun CJ, Sung CJ, hu DL, Law CK. Response of counterflow premixed and diffusion flames to strain rate variations at reduced and elevated pressures. Symposium (International) on Combustion 1996;26(1):1111–20.
[37] Serrano C, Hernnandez JJ, Mandilas C, Sheppard CGW, Woolley R. Laminar burning behaviour of biomass gasification-derived producer gas. International Journal of Hydrogen Energy 2008;33(2):851–62.
[38] Law CK, Sung CJ. Structure, aerodynamics, and geometry of premixed flamelets. Progress in Energy and Combustion Science 2000;26(4–6):459–505.
[39] Clavin P. Dynamic behavior of premixed flame fronts in laminar and turbulent flows. Progress in Energy and Combustion Science 1985;11(1):1–59.